AIAA 80-0688R

Analysis of Simply-Supported Orthotropic Plates Subject to Static and Dynamic Loads

A. L. Dobyns*
Boeing Military Airplane Company, Seattle, Wash.

Equations are presented for the analysis of simply-supported orthotropic plates subjected to static and dynamic loading conditions. Transient loading conditions considered include sine, rectangular, and triangular pulses, and pulses representative of high explosive blast and nuclear blast. These pulses can be applied as a uniform load over the panel, a concentrated load, a uniform load applied over a small rectangular area, and a cosine loading applied over a small rectangular area. A method for the analysis of low velocity impact is also presented.

Introduction

THE analysis of laminated composite plates subject to static and dynamic loads has received widespread attention in recent years. Lekhnitskii,[1] Ambartsumyan,[2] Jones,[3] Whitney and Leissa,[4] and Ashton and Whitney,[5] have presented analyses for laminated plates with infinite normal shear rigidity while Whitney and Pagano[6] have presented an extension of Mindlin's[7] beam theory to laminated plates with normal shear deformations. Papers dealing with the response of plates to dynamic loading have been less in evidence. Meirovitch[8] and Warburton[9] presented the response of isotropic plates to dynamic loading while Yu,[10] and Sun and Whitney[11,12] have analyzed the response of anisotropic plates in cylindrical bending using Mindlin's[7] method to account for normal shear stiffness. Sun and Chattopadhyay[13] used the plate equations developed by Whitney and Pagano[6] to analyze a specially orthotropic plate subject to a center impact.

This paper considers the analysis of thin simply supported orthotropic plates subjected to static and dynamic loading. The specially orthotropic form of the equations of motion is used instead of the more general equations incorporating bending-stretching coupling used in Refs. 10-12 in order to obtain solutions that are generally applicable to engineering problems.

The paper presents the governing equations for an orthotropic rectangular plate and obtains static solutions for several loading cases. The vibration frequencies and mode shapes are then determined and solutions for plate deflections, bending strains, and normal shear forces due to several transient loads are obtained. It is seen that the dynamic solution is closely akin to the static solution and requires only a small additional effort to obtain. A solution for plate impact loading is then given, followed by several examples of static and dynamic loads.

Governing Equations

The plate equations developed by Whitney and Pagano[6] are used as they include the effect of transverse shear deformations. The assumed displacement field is given by

$$u=u^0(x,y,t)+z\psi_x(x,y,t) \quad v=v^0(x,y,t)+z\psi_y(x,y,t)$$

$$w=w(x,y,t) \tag{1}$$

Where u^0, v^0, and w are the plate displacements in the x, y, and z directions at the plate midplane and ψ_x and ψ_y are the shear rotations in the x and y directions. Taking the equations of motion developed by Whitney and Pagano, reducing them to specially orthotropic form ($B_{ij}=0$, $A_{16}=A_{26}=D_{16}=D_{26}=0$), and adding the uniform initial stress resultants N_x^0 and N_y^0 as discussed by Sun and Chattopadhyay[13] and a foundation stiffness K results in

$$D_{11}\psi_{x,xx}+D_{66}\psi_{x,yy}+(D_{12}+D_{66})\psi_{y,xy}-\kappa A_{55}\psi_x-\kappa A_{55}w_{,x}+m_x=I\ddot{\psi}_x \tag{2a}$$

$$(D_{12}+D_{66})\psi_{x,xy}+D_{66}\psi_{y,xx}+D_{22}\psi_{y,yy}-\kappa A_{44}\psi_y-\kappa A_{44}w_{,y}+m_y=I\ddot{\psi}_y \tag{2b}$$

$$\kappa A_{55}\psi_{x,x}+(\kappa A_{55}+N_x^0)w_{,xx}+\kappa A_{44}\psi_{y,y}+(\kappa A_{44}+N_y^0)w_{,yy}+p_z+Kw=P\ddot{w} \tag{2c}$$

where differentiation with respect to x or y is denoted by a comma while differentiation with respect to time is denoted by a dot. The distributed loads p_z, m_x, m_y are as given by Sun and Whitney.[11] Also, κ is a shear correction factor introduced by Mindlin[7] and is popularly taken to be $\pi^2/12$, and the stiffness and inertias are given by

$$(A_{ij},D_{ij})=\int_{-h/2}^{h/2}Q_{ij}(1,z^2)\,dz \qquad i,j=1,2,6$$

$$A_{ij}=\int_{-h/2}^{h/2}C_{ij}\,dz \qquad i,j=4,5$$

$$(P,I)=\int_{-h/2}^{h/2}\rho(1,z^2)\,dz \tag{3}$$

The Q_{ij} are reduced in-plane stiffnesses for plane stress and C_{ij} are transverse shear stiffnesses, as defined in Ref. 6. By defining B_{ij} as zero the equations of motion given in Ref. 6 decouple into two independent groups, of which only the group concerned with transverse displacement is considered here.

This paper is concerned with a simply supported rectangular plate of uniform thickness with dimensions a and b for which the boundary conditions are given by

$$w=\psi_{x,x}=0 \text{ at } x=0,a$$

$$w=\psi_{y,y}=0 \text{ at } y=0,b \tag{4}$$

Presented as Paper 80-0688 at the AIAA/ASME/ASCE/AHS 21st Structures, Structural Dynamics and Materials Conference, Seattle, Wash., June 4-6, 1980; submitted June 5, 1980; revision received Nov. 18, 1980.

*Research Engineer, Advanced Composites Development Group. Member AIAA.

Static Loading

For a static load, solutions to Eq. (2) that satisfy the boundary conditions Eq. (4) are given by

$$\Psi_x = A_{mn}\cos(m\pi x/a)\sin(n\pi y/b)$$

$$\Psi_y = B_{mn}\sin(m\pi x/a)\cos(n\pi y/b)$$

$$W = C_{mn}\sin(m\pi x/a)\sin(n\pi y/b) \tag{5}$$

with the loading function given by

$$p_z = q_{mn}\sin(m\pi x/a)\sin(n\pi y/b) \tag{6}$$

where q_{mn} are the terms of a Fourier series representation of the load. Substituting Eqs. (5) and (6) into the equations of motion Eqs. (2) produces

$$\begin{bmatrix} L_{11} & L_{12} & L_{13} \\ L_{12} & L_{22} & L_{23} \\ L_{13} & L_{23} & L_{33} \end{bmatrix} \begin{Bmatrix} A_{mn} \\ B_{mn} \\ C_{mn} \end{Bmatrix} = \begin{Bmatrix} 0 \\ 0 \\ q_{mn} \end{Bmatrix} \tag{7}$$

where

$$L_{11} = D_{11}(m\pi/a)^2 + D_{66}(n\pi/b)^2 + \kappa A_{55}$$

$$L_{12} = (D_{12} + D_{66})(m\pi/a)(n\pi/b)$$

$$L_{13} = \kappa A_{55}(m\pi/a)$$

$$L_{22} = D_{66}(m\pi/a)^2 + D_{22}(n\pi/b)^2 + \kappa A_{44}$$

$$L_{23} = \kappa A_{44}(n\pi/b)$$

$$L_{33} = (\kappa A_{55} + N_x^0)(m\pi/a)^2 + (\kappa A_{44} + N_y^0)(n\pi/b)^2 + K$$

solving Eq. (7) for A_{mn}, B_{mn}, C_{mn}, results in

$$A_{mn} = \frac{(L_{12}L_{23} - L_{22}L_{13})q_{mn}}{\det}$$

$$B_{mn} = \frac{(L_{12}L_{13} - L_{11}L_{23})q_{mn}}{\det}$$

$$C_{mn} = \frac{(L_{11}L_{22} - L_{12}^2)q_{mn}}{\det} \tag{8}$$

where det is the determinant of the matrix in Eq. (7). Using Eqs. (5) and (8) with the constitutive equations from Ref. 6, the strains and shear forces at any point in the plate may be calculated as

$$w = \sum_m \sum_n C_{mn}\sin\frac{m\pi x}{a}\sin\frac{n\pi y}{b}$$

$$\epsilon_x = z\psi_{x,x} = -z\sum_m \sum_n A_{mn}\frac{m\pi}{a}\sin\frac{m\pi x}{a}\sin\frac{n\pi y}{b}$$

$$\epsilon_y = z\psi_{y,y} = -z\sum_m \sum_n B_{mn}\frac{n\pi}{a}\sin\frac{m\pi x}{a}\sin\frac{n\pi y}{b}$$

$$\gamma_{xy} = z(\psi_{x,y} + \psi_{y,x})$$

$$= z\sum_m \sum_n \left(A_{mn}\frac{n\pi}{b} + B_{mn}\frac{m\pi}{a}\right)\cos\frac{m\pi x}{a}\cos\frac{n\pi y}{b}$$

$$Q_x = \kappa A_{55}(W_{,x} + \psi_x) = \sum_m \sum_n kA_{55}\left(C_{mn}\frac{m\pi}{a} + A_{mn}\right)$$

$$\times\cos\frac{m\pi x}{a}\sin\frac{n\pi y}{b}$$

$$Q_y = \kappa A_{44}(W_{,y} + \psi_y) = \sum_m \sum_n kA_{44}\left(C_{mn}\frac{n\pi}{b} + B_{mn}\right)$$

$$\times\sin\frac{m\pi x}{a}\cos\frac{n\pi y}{b} \tag{9}$$

where Σ_m indicates a summation for $m = 1$ to ∞.

The terms in the Fourier series representation of the load may be determined from [14]

$$q_{mn} = \frac{4}{ab}\int_0^a \int_0^b p(x,y)\sin\frac{m\pi x}{a}\sin\frac{n\pi y}{b}\,dx\,dy \tag{10}$$

For a uniform load q_{mn} becomes

$$q_{mn} = (4p_z/mn\pi^2)(1-\cos m\pi)(1-\cos n\pi) \tag{11}$$

where p_z is the pressure.

For a concentrated load located at the point ζ, η, q_{mn} is

$$q_{mn} = \frac{4P_z}{ab}\sin\frac{m\pi\zeta}{a}\sin\frac{n\pi\eta}{b} \tag{12}$$

where P_z is the total load. For a uniform load over the rectangular area u, v with center at ζ, η, as shown in Fig. 1, q_{mn} is

$$q_{mn} = \frac{16P_z}{\pi^2 mnuv}\sin\frac{m\pi\zeta}{a}\sin\frac{n\pi\eta}{b}\sin\frac{m\pi u}{2a}\sin\frac{n\pi v}{2b} \tag{13}$$

For a cosine loading over the rectangular area u, v, as shown in Fig. 1, q_{mn} is

$$q_{mn} = \frac{4P_z\sin\frac{n\pi\eta}{b}\sin\frac{m\pi\zeta}{a}\cos\frac{n\pi v}{2b}\cos\frac{m\pi u}{2a}}{abu^2v^2\left(\frac{n}{b}-\frac{1}{v}\right)\left(\frac{n}{b}+\frac{1}{v}\right)\left(\frac{m}{a}-\frac{1}{u}\right)\left(\frac{m}{a}+\frac{1}{u}\right)}$$

$$\frac{n}{b} \neq \frac{1}{v},\ \frac{m}{a} \neq \frac{1}{u} \tag{14}$$

$$q_{mn} = 0 \qquad \frac{n}{b} = \frac{1}{v},\ \frac{m}{a} = \frac{1}{u}$$

Other static loading distributions can be analyzed by inserting the appropriate relation into Eq. (10).

Dynamic Loading

The frequency of natural vibration may be computed by assuming for displacements

$$\psi_x = \Psi_x e^{i\omega t},\quad \psi_y = \Psi_y e^{i\omega t},\quad w = We^{i\omega t} \tag{15}$$

where Ψ_x, Ψ_y, and W are given by Eq. (5). Substituting the assumed displacements Eq. (15) into the equations of motion Eq. (2) results in

$$D_{11}\Psi_{x,xx_{mn}} + D_{66}\Psi_{x,yy_{mn}} + (D_{12} + D_{66})\Psi_{y,xy_{mn}}$$

$$-\kappa A_{55}\Psi_{x_{mn}} - \kappa A_{55}W_{,x_{mn}} = -\omega_{mn}^2 I\Psi_{x_{mn}} \tag{16a}$$

$$(D_{12} + D_{66})\Psi_{x,xy_{mn}} + D_{66}\Psi_{y,xx_{mn}} + D_{22}\Psi_{y,yy_{mn}}$$

$$-\kappa A_{44}\Psi_{y_{mn}} - \kappa A_{44}W_{,y_{mn}} = -\omega_{mn}^2 I\Psi_{y_{mn}} \tag{16b}$$

$$\kappa A_{55}\Psi_{x,x_{mn}} + (\kappa A_{55} + N_x^0)\, W_{,xx_{mn}} + \kappa A_{44}\Psi_{y,y_{mn}}$$
$$+ (\kappa A_{44} + N_y^0)\, W_{,yy_{mn}} + KW_{mn} = -\omega_{mn}^2 PW_{mn} \qquad (16c)$$

Substituting Eq. (5) and its derivatives into Eq. (16) results in a set of homogeneous equations that may be solved for the natural frequencies of vibration.

$$\begin{bmatrix} L'_{11} & L_{12} & L_{13} \\ L_{12} & L'_{22} & L_{23} \\ L_{13} & L_{23} & L'_{33} \end{bmatrix} \begin{Bmatrix} A'_{mn} \\ B'_{mn} \\ C'_{mn} \end{Bmatrix} = \begin{Bmatrix} 0 \\ 0 \\ 0 \end{Bmatrix} \qquad (17)$$

where L_{12}, L_{13}, etc. are given by Eq. (7) and L'_{11}, L'_{22}, and L'_{33} are given by

$$L'_{11} = L_{11} - \omega_{mn}^2 I,\quad L'_{22} = L_{22} - \omega_{mn}^2 I,\quad L'_{33} = L_{33} - \omega_{mn}^2 P \qquad (18)$$

Three eigenvalues and their respective eigenvectors result from Eq. (17) for each m, n pair. If the rotational inertia (I) can be neglected, then L_{11} and L_{22} may be used in Eq. (17) instead of L'_{11} and L'_{22}. Mindlin[7] has shown that rotatory inertia has little effect in isotropic plates and it is popularly assumed that the same holds true for orthotropic plates. In that case only one eigenvalue and its eigenvector results for each m, n, as given by

$$\omega_{mn}^2 = (QL_{33} + 2L_{12}L_{23}L_{13} - L_{22}L_{13}^2 - L_{11}L_{13}^2)/(PQ)$$
$$Q = L_{11}L_{22} - L_{12}^2 \qquad (19)$$

The eigenvectors associated with the natural frequencies given by Eq. (19) are

$$A'_{mn} = \frac{L_{12}L_{23} - L_{22}L_{13}}{L_{11}L_{22} - L_{12}^2} C'_{mn},\quad B'_{mn} = \frac{L_{12}L_{13} - L_{11}L_{23}}{L_{11}L_{22} - L_{12}^2} C'_{mn} \qquad (20)$$

when normalized to C'_{mn}.

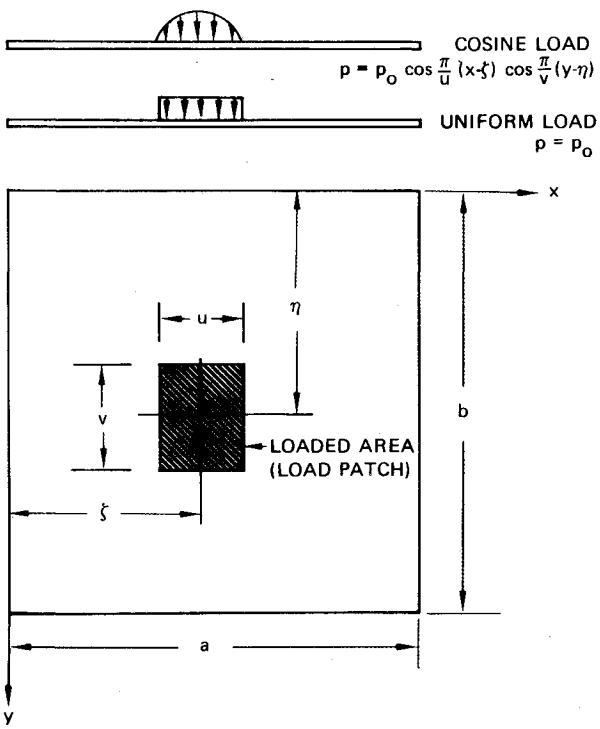

Fig. 1 Location and shape of loaded area.

The orthogonality condition for the principal modes is given by[10,11]

$$(\omega_{mn}^2 - \omega_{pq}^2)\int_0^a\int_0^b (PW_{mn}W_{pq} + I\Psi_{x_{mn}}\Psi_{x_{pq}}$$
$$+ I\Psi_{y_{mn}}\Psi_{y_{pq}})\,dxdy = 0 \qquad (21)$$

so that if $m, n \neq p, q$ the integral is zero.

The solution to the equations of motion can be separated into a function of position and a function of time as follows:

$$\psi_x(x,y,t) = \sum_m\sum_n \Psi_{x_{mn}}(x,y)\,T_{mn}(t)$$
$$\psi_y(x,y,t) = \sum_m\sum_n \Psi_{y_{mn}}(x,y)\,T_{mn}(t)$$
$$w(x,y,t) = \sum_m\sum_n W_{mn}(x,y)\,T_{mn}(t) \qquad (22)$$

where $T_{mn}(t)$ is a time dependent generalized coordinate. Substituting Eq. (22) into the equations of motion Eqs. (2) and using Eq. (16) gives

$$-\sum_m\sum_n \omega_{mn}^2 \Psi_{x_{mn}} T_{mn} + \frac{m_x}{I} = \sum_m\sum_n \Psi_{x_{mn}}\ddot{T}_{mn}$$
$$-\sum_m\sum_n \omega_{mn}^2 \Psi_{y_{mn}} T_{mn} + \frac{m_y}{I} = \sum_m\sum_n \Psi_{y_{mn}}\ddot{T}_{mn}$$
$$-\sum_m\sum_n \omega_{mn}^2 W_{mn} T_{mn} + \frac{p_z}{P} = \sum_m\sum_n W_{mn}\ddot{T}_{mn} \qquad (23)$$

The distributed loads m_x, m_y, and p_z may be expanded in terms of the generalized forces $Q_{mn}(t)$ as

$$\frac{m_x}{I} = \sum_m\sum_n Q_{mn}(t)\,\Psi_{x_{mn}}(x,y)$$
$$\frac{m_y}{I} = \sum_m\sum_n Q_{mn}(t)\,\Psi_{y_{mn}}(x,y)$$
$$\frac{p_z}{P} = \sum_m\sum_n Q_{mn}(t)\,W_{mn}(x,y) \qquad (24)$$

$Q_{mn}(t)$ may be solved for by multiplying the first equation by $I\Psi_x$, the second by $I\Psi_y$, and the third by PW, adding all three and integrating over the plate area.[10,11] Due to the orthogonality condition Eq. (21), we may drop the summation, resulting in

$$Q_{mn}(t) = \frac{\int_0^a\int_0^b (m_x\Psi_{x_{mn}} + m_y\Psi_{y_{mn}} + p_z W_{mn})\,dxdy}{\int_0^a\int_0^b (\Psi_{x_{mn}}^2 I + \Psi_{y_{mn}}^2 I + W_{mn}^2 P)\,dxdy} \qquad (25)$$

Putting Eq. (24) into Eq. (23) gives, for any m, n

$$\ddot{T}_{mn}(t) + \omega_{mn}^2 T_{mn}(t) = Q_{mn}(t) \qquad (26)$$

For zero initial displacement and velocity, the solution to Eq. (26) is

$$T_{mn}(t) = \frac{1}{\omega_{mn}}\int_0^t Q_{mn}(\tau)\sin\omega_{mn}(t-\tau)\,d\tau \qquad (27)$$

The solution for w, ψ_x, and ψ_y is obtained by substituting Eqs. (5), (20), (25), and (27) into Eq. (22).

For cases in which rotatory inertia can be neglected, relatively simple relations for w, ψ_x, and ψ_y can be determined. If $m_x = m_y = I = 0$, then the generalized force $Q_{mn}(t)$ may be expressed as

$$Q_{mn}(t) = \frac{4}{PabC'_{mn}} \int_0^a \int_0^b p_z(x,y) \sin\frac{m\pi x}{a} \sin\frac{n\pi y}{b}\, dx dy \quad (28)$$

Comparing Eq. (28) with the Fourier series for static loading Eq. (10), it can be seen that

$$Q_{mn}(t) = (q_{mn}/PC'_{mn}) \quad (29)$$

Using Eq. (29) with Eqs. (5), (20), (22), (25), and (27) results in expressions for the deformations in a plate under a transverse loading.

$$w(x,y,t) = \frac{1}{P} \sum_m \sum_n \frac{q_{mn} \sin(m\pi x/a) \sin(n\pi y/b)}{\omega_{mn}} \times \int_0^t F(\tau) \sin\omega_{mn}(t-\tau)\, d\tau \quad (30a)$$

$$\psi_x(x,y,t) = \frac{1}{P} \sum_m \sum_n \left(\frac{L_{12}L_{23} - L_{22}L_{13}}{L_{11}L_{22} - L_{12}^2}\right) \times \frac{q_{mn} \cos(m\pi x/a) \sin(n\pi y/b)}{\omega_{mn}} \int_0^t F(\tau) \sin\omega_{mn}(t-\tau)\, d\tau \quad (30b)$$

$$\psi_y(x,y,t) = \frac{1}{P} \sum_m \sum_n \left(\frac{L_{12}L_{13} - L_{11}L_{23}}{L_{11}L_{22} - L_{12}^2}\right) \times \frac{q_{mn} \sin(m\pi x/a) \cos(n\pi y/b)}{\omega_{mn}} \int_0^t F(\tau) \sin\omega_{mn}(t-\tau)\, d\tau \quad (30c)$$

Bending strains ϵ_x, ϵ_y, γ_{xy} and normal shear forces Q_x and Q_y at any point in the plate may be computed from Eqs. (30) using Eq. (9).

The convolution integral in Eq. (30) has been solved analytically for several commonly encountered forcing functions; a sine pulse, a step pulse, a triangular pulse, a stepped triangular pulse, and an exponential pulse, where the pulse definition is given in Fig. 2. For a sine pulse the forcing function $F(t)$ and the convolution integral are

$$F(t) = F_0 \sin(\pi t/t_1) \qquad 0 \le t \le t_1$$

$$F(t) = 0 \qquad t > t_1$$

$$\int_0^t F(t) \sin\omega_{mn}(t-\tau)\, d\tau = \frac{F_0 t_1 [\pi \sin\omega_{mn} t - \omega_{mn} t_1 \sin(\pi t/t_1)]}{(\pi^2 - t_1^2 \omega_{mn}^2)} \qquad 0 \le t \le t_1$$

$$\int_0^t F(t) \sin\omega_{mn}(t-\tau)\, d\tau = \frac{F_0 \pi t_1 [\sin\omega_{mn} t + \sin\omega_{mn}(t-t_1)]}{(\pi^2 - t_1^2 \omega_{mn}^2)} \qquad t > t_1 \quad (31)$$

For a stepped pulse

$$F(t) = F_0 \qquad 0 \le t \le t_1$$

$$F(t) = 0 \qquad t > t_1$$

$$\int_0^t F(t) \sin\omega_{mn}(t-\tau)\, d\tau = \frac{F_0}{\omega_{mn}} (1 - \cos\omega_{mn} t) \qquad 0 \le t \le t_1$$

$$\int_0^t F(t) \sin\omega_{mn}(t-\tau)\, d\tau = \frac{F_0}{\omega_{mn}} [\cos\omega_{mn}(t-t_1) - \cos\omega_{mn} t] \qquad t > t_1 \quad (32)$$

For a triangular pulse

$$F(t) = F_0(1 - t/t_1) \qquad 0 \le t \le t_1$$

$$F(t) = 0 \qquad t > t_1$$

$$\int_0^t F(t) \sin\omega_{mn}(t-\tau)\, d\tau = \frac{F_0}{\omega_{mn}} \left[1 - \cos\omega_{mn} t + \frac{1}{\omega_{mn} t_1} \sin\omega_{mn} t - t/t_1\right] \qquad 0 \le t \le t_1$$

$$\int_0^t F(t) \sin\omega_{mn}(t-\tau)\, d\tau = F_0 \left[-\frac{1}{\omega_{mn}} \cos\omega_{mn} t + \frac{2}{\omega_{mn}^2 t_1} \cos\omega_{mn}(t - t_1/2) \sin\omega_{mn}(t_1/2)\right] \qquad t > t_1 \quad (33)$$

The stepped triangular pulse can be used to simulate a nuclear blast loading where the pressure pulse consists of a

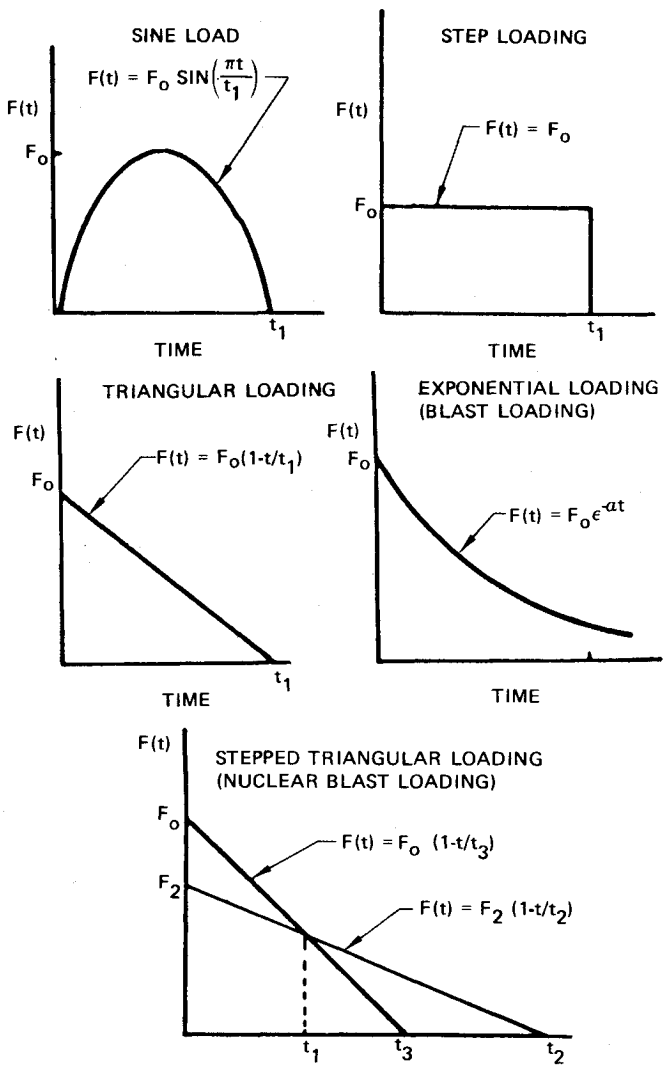

Fig. 2 Load pulse shapes.

long duration phase of several seconds due to the overpressure and a short duration phase of a few milliseconds due to shock wave reflection. The short duration phase has twice the pressure of the long duration phase.[15] For a stepped triangular pulse the equations are

$$F(t)=F_0(1-t/t_3) \qquad 0\le t\le t_1$$

$$F(t)=F_2(1-t/t_2) \qquad t_1\le t\le t_2$$

$$F(t)=0 \qquad t>t_2$$

$$\int_0^t F(t)\sin\omega_{mn}(t-\tau)\,d\tau=\frac{F_0}{\omega_{mn}}\left[1-\cos\omega_{mn}t+\frac{1}{\omega_{mn}t_3}\sin\omega_{mn}t-t/t_3\right] \qquad 0\le t\le t_1$$

$$\int_0^t F(t)\sin_{\omega mn}(t-\tau)\,d\tau=F_0\left[\frac{1}{\omega_{mn}}(1-t_1/t_3)\cos\omega_{mn}(t-t_1)-\frac{1}{\omega_{mn}}\cos\omega_{mn}t-\frac{1}{\omega_{mn}^2t_3}\sin\omega_{mn}(t-t_1)+\frac{1}{\omega_{mn}^2t_3}\sin\omega_{mn}t\right]$$
$$+F_2\left[\frac{1}{\omega_{mn}}\left(1-\frac{t}{t_2}\right)-\frac{1}{\omega_{mn}}(1-t_1/t_2)\cos\omega_{mn}(t-t_1)+\frac{1}{\omega_{mn}^2t_2}\sin\omega_{mn}(t-t_1)\right] \qquad t_1\le t\le t_2$$

$$\int_0^t F(t)\sin\omega_{mn}(t-\tau)\,d\tau=F_0\left[\frac{1}{\omega_{mn}}\left(1-\frac{t_1}{t_3}\right)\cos\omega_{mn}(t-t_1)-\frac{1}{\omega_{mn}}\cos\omega_{mn}t+\frac{1}{\omega_{mn}^2t_3}\{\sin\omega_{mn}t-\sin\omega_{mn}(t-t_1)\}\right]$$
$$+F_2\left[\frac{1}{\omega_{mn}}\left(\frac{t_1}{t_2}-1\right)\cos\omega_{mn}(t-t_1)-\frac{1}{\omega_{mn}^2t_2}\{\sin\omega_{mn}(t-t_2)-\sin\omega_{mn}(t-t_1)\}\right] \qquad t>t_2 \qquad (34)$$

The exponential pulse may be used to simulate a high explosive blast loading if the decay parameter α is adjusted to approximate the pressure curve from a blast test. For the exponential pulse the equations are

$$F(t)=F_0e^{-\alpha t}$$

$$\int_0^t F(t)\sin\omega_{mn}(t-\tau)\,d\tau=\frac{F_0[\omega_{mn}e^{-\alpha t}+\alpha\sin\omega_{mn}t-\omega_{mn}\cos\omega_{mn}t]}{(\alpha^2+\omega_{mn}^2)} \qquad (35)$$

Impact Loading

The response of a rectangular orthotropic panel to impact loading may be computed from the transient response Eq. (30) by computing the impact force from the deceleration of the impactor mass. Timoshenko[16] obtained the equation for a rigid impact between a mass and a beam as

$$v_0t-(1/m)\int_0^t dt\int_0^t F\,dt=w_1(c) \qquad (36)$$

where v_0 is the initial velocity of the impactor with mass m, $w_1(c)$ the transient response of the structure at the impacted point (c) as a function of time, and F the contact force. Equation (36) may be extended to include the effect of a flexible impactor as given by Goldsmith.[17]

$$\alpha=w_2-w_1(c)=v_0t-(1/m)\int_0^t dt\int_0^t F\,dt-w_1(c) \qquad (37)$$

where α is the difference between the displacement of the striker (w_2) and the deflection of the structure at the contact point $w_1(c)$, as shown in Fig. 3. Hertz's law of contact,[17] that gives a relationship between the contact force and the deformation as

$$F=k_2\alpha^{3/2} \qquad (38)$$

can be substituted into Eq. (37) to obtain an equation for the impact response of a plate

$$\left(\frac{F}{k_2}\right)^{2/3}=v_0t-(1/m)\int_0^t dt\int_0^t F\,dt-w_1(c) \qquad (39)$$

where

$$k_2=\frac{4\sqrt{R_1}}{3\pi(\delta_1+\delta_2)} \qquad (40)$$

R_1 is the impactor radius and δ_1, and δ_2 functions of the Poisson's ratio and modulus E of the impactor and the plate, given by

$$\delta_i=(1-\mu_i^2)/E_i\pi \qquad (41)$$

Since Eq. (39) is a nonlinear equation, it must be solved numerically as discussed by Sun and Chattopadhyay.[13] Sun and Chattopadhyay obtained a solution for the response of an orthotropic plate to center impact idealized as a concentrated load, that resulted in the prediction of an infinite normal shear force at the impact point. Using Eq. (30) with Eq. (13) or (14), the impact load may be idealized as a uniform load over a small rectangular area or as a cosine shaped load over a small rectangular area, which allows more realistic values for the normal shear force to be computed.

Examples of Static and Dynamic Loading

Figure 4 shows a plot of the variation of bending strain and normal shear force across the center of a plate loaded by a uniform load over a small area. The maximum shear load

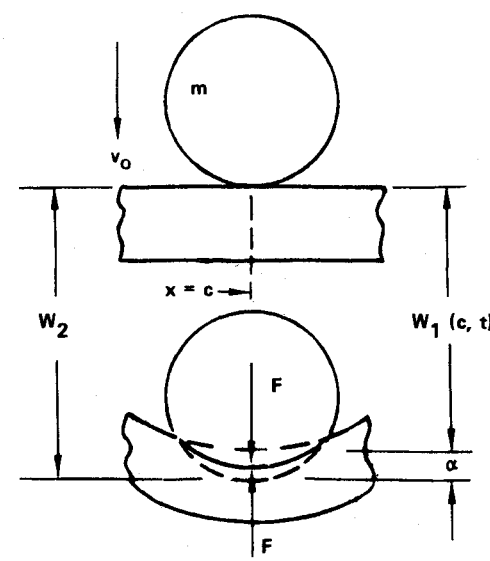

Fig. 3 Central transverse impact of a rigid body with a curved contact surface.

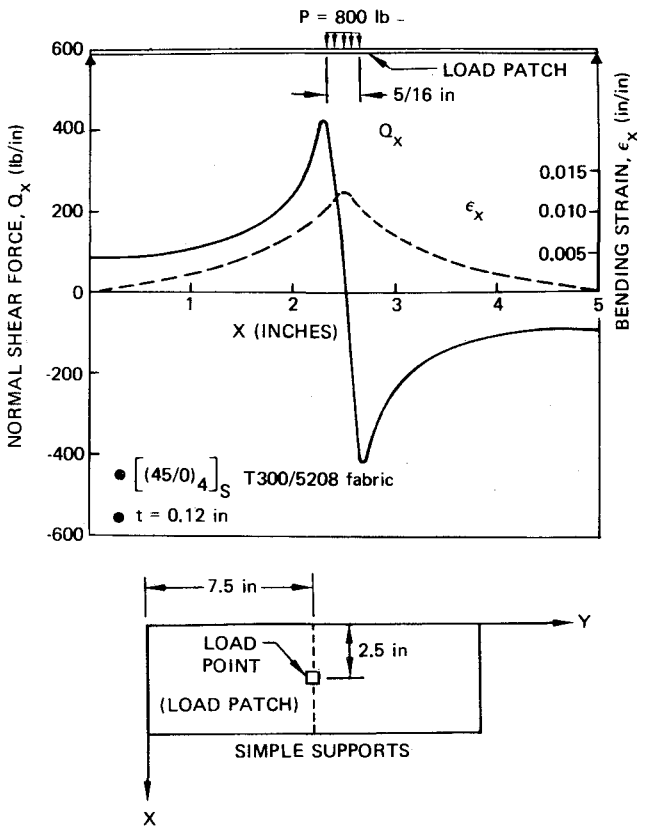

Fig. 4 Normal shear force and bending strain distribution of an impacted plate.

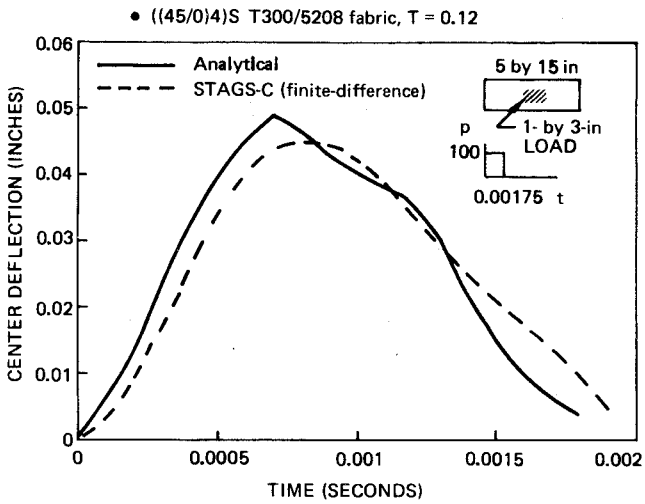

Fig. 5 Comparison of STAGS-C with analytical method.

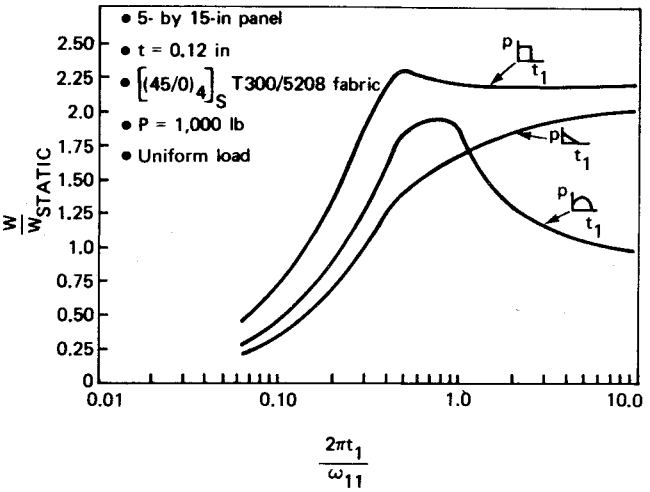

Fig. 6 Effect of load pulse length on dynamic magnification factor.

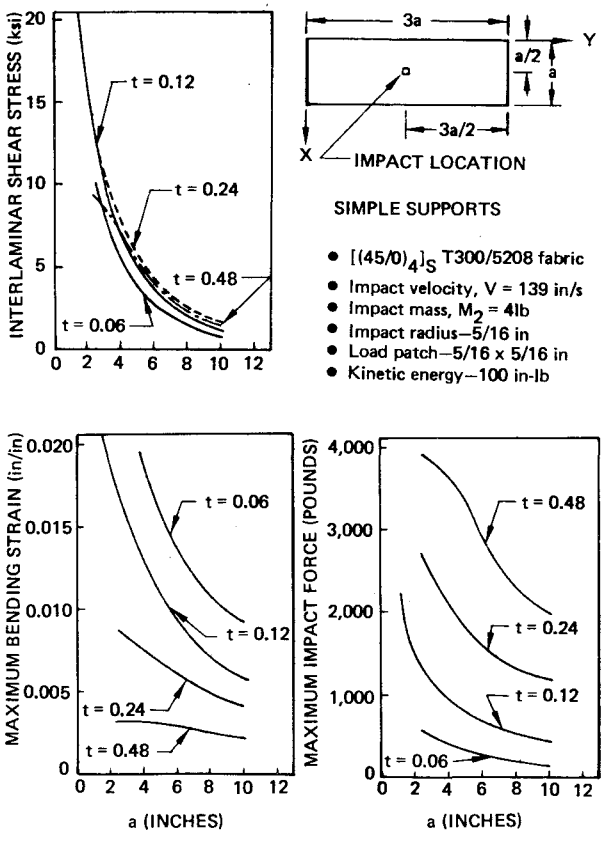

Fig. 7 Effect of size on solid laminate panel response.

occurs at the edge of the load patch, as would be expected from beam theory.

Figure 5 shows a plot of the center deflection as a function of time for a plate loaded by a step pulse, analyzed by the STAGS-C finite-difference program and by the method given in this paper. The correlation between the two methods is good, although it deteriorates when the load is increased enough to produce deflections greater than the panel thickness. At a load of 1000 lb the STAGS-C program gives a predicted deflection of 0.255 in. while the analytical method gives a prediction of 0.493 in., indicating that large deflection effects are becoming too important to ignore.

Figure 6 shows the predicted dynamic magnification factor on panel center deflection for three types of loading pulse, as a function of the pulse length. It can be seen that the response to the step pulse and the sine pulse reaches a maximum when the pulse length is near the longest natural period of the plate (lowest natural frequency) while the response to the triangular pulse continues to increase with pulse length.

Several studies have been conducted on the response of graphite/epoxy solid laminate and honeycomb plates using the method developed by Sun and Chattopadhyay,[13] modified to apply the impact load as a uniform load over a small rectangular area. This allows a more realistic value of the normal shear force and interlaminar shear stress to be computed than the concentrated load originally used. Figure 7 shows the effect of panel size and thickness on the maximum interlaminar shear stress, bending strain, and impact force for a constant impact energy on a solid laminate panel. It can be seen that the plate thickness has only a small effect on the interlaminar shear stress but a large effect on the bending

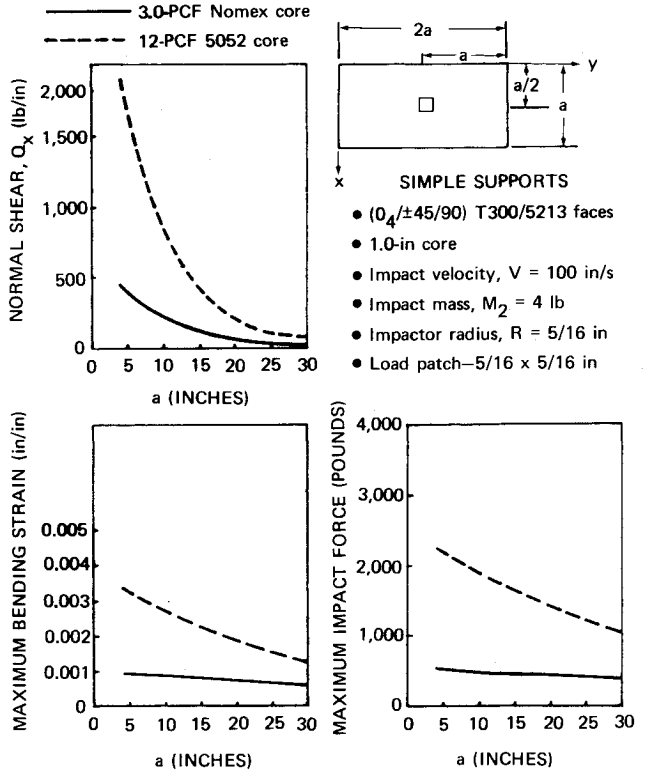

Fig. 8 Effect of panel size and core shear stiffness on sandwich panel response.

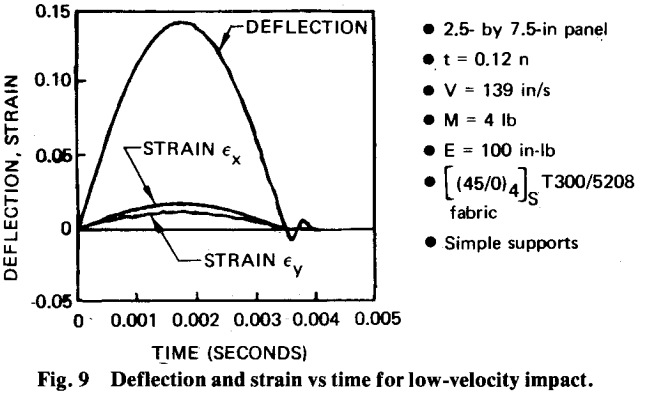

Fig. 9 Deflection and strain vs time for low-velocity impact.

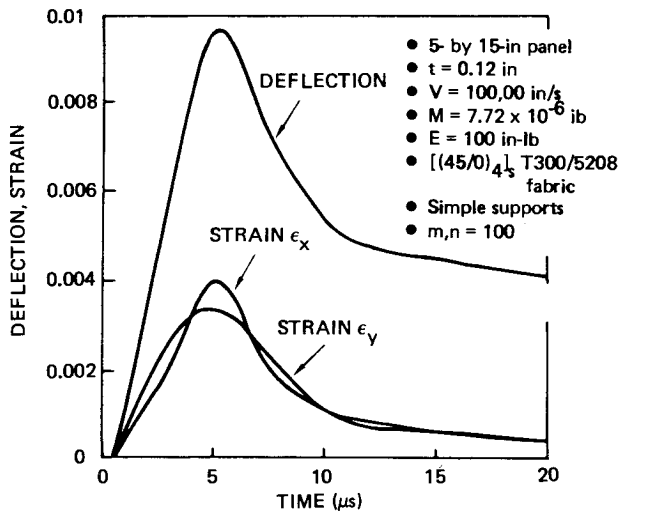

Fig. 10 Deflection and strain vs time for high-velocity impact.

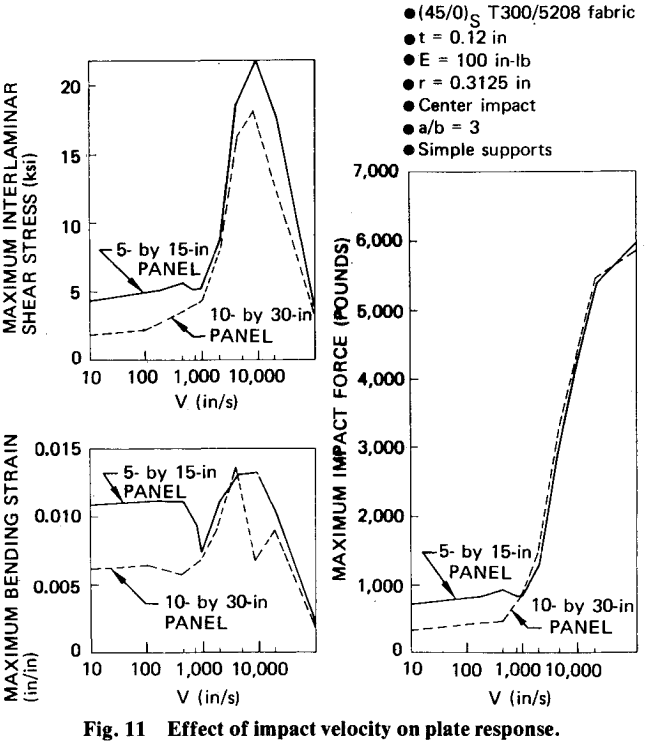

Fig. 11 Effect of impact velocity on plate response.

strain and impact force, while the plate size has a large effect on all three parameters.

Figure 8 shows a similar set of plots for a honeycomb sandwich panel with two different core shear stiffnesses, using the Hertz force-deformation relation. The Hertz relation, given by Eq. (38), is not correct for honeycomb panels since it predicts an increasing stiffness with increasing deformation, whereas the honeycomb shows a decreasing stiffness with increasing deformation, due to core crushing. The Hertz relation was used to get preliminary results until a more correct force-deformation equation could be determined. In the figure, the 3.0 pcf Nomex core has a shear stiffness of only 35.8 MPa (5200 psi) while the 12 pcf 5052 core has a shear stiffness of 1158 MPa (168,000 psi), so that the panel made with Nomex core is much more flexible than the panel with aluminum core. The result is that the Nomex panel is much less sensitive to panel size than the panel with the stiffer 5052 core, since the flexible panel allows more deformation in the local impact region, both by core shear deformation and by core crushing.

A study has been made on the effect of impact velocity on the response of a solid laminate graphite/epoxy panel. Figure 9 shows the center deflection and strain vs time response for a panel impacted at 3.5 m/s (139 in./s) while Fig. 10 shows the response of a panel impacted at 2540 m/s (100,000 in./s), with an impact energy of 11.3 J (100 in.-lb) in both cases. The low velocity impact response appears to be very similar to the static response in that the peak deflection and strain occur at the same time and the deflection shape is similar to the static deflection shape. It was necessary to include a large number of mode shapes in the solution for the higher impact velocities to obtain good results. The solution shown in Fig. 10 required 100 terms in each direction to obtain good strain values. It required 400 terms in each direction to obtain good transverse shear values. Sun and Lai[18] have shown that the general equations used in this analysis are valid for stress wave phenomena, which lends credence to the results shown for the 2540 m/s (100,000 in./s) impact. Figure 11 shows a plot of plate response vs impact velocity for two panel sizes. At low impact velocities there is a large difference in response for the two panel sizes as would be expected from the static loading results while at higher velocities the panel size has only a small

Table 1 Comparison of test and computed delamination size

Impact energy J.	(in.-lb)	Delamination size, mm (in.) F_{IS} allowable = 68.9 MPa	(10,000 lb/in.^{2})	F_{IS} allowable = 34.5 MPa	(5000 lb/in.^{2})	Test
15.8	(140)	16.7	(0.66)	37.1	(1.46)	41.9 (1.65)
11.3	(100)	12.2	(0.48)	28.4	(1.12)	31.0 (1.22)
6.3	(60)	10.2	(0.40)	22.3	(0.88)	22.1 (0.87)

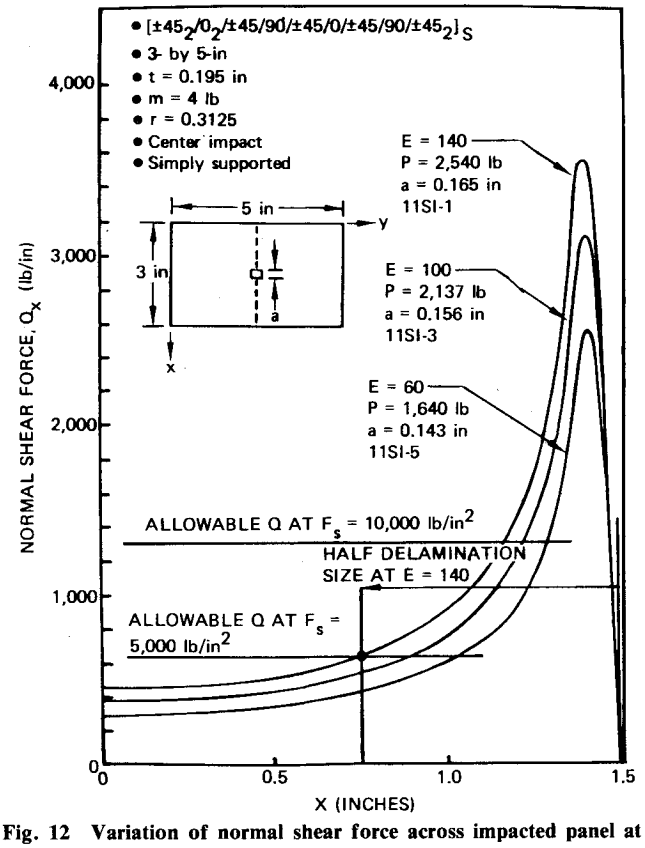

Fig. 12 Variation of normal shear force across impacted panel at $y = 63.5$ mm (2.5 in.).

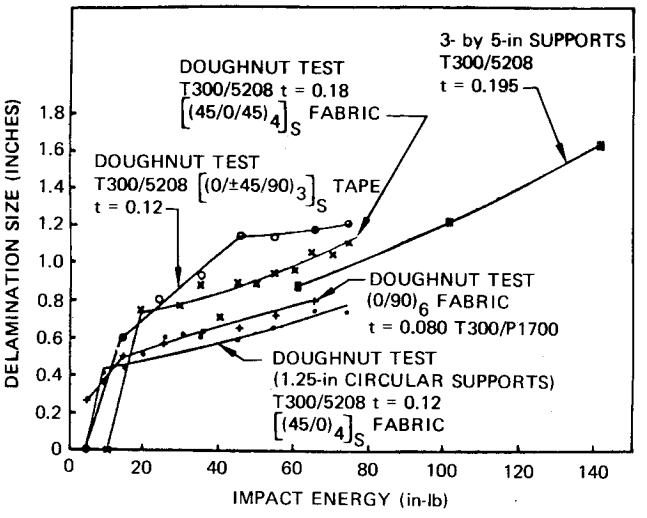

Fig. 13 Relationship of damage size to impact energy for graphite panels.

effect. It appears that at impact velocities greater than 25.4 m/s (1000 in./s) the panel deformation is limited to the impact region, so that panel size and boundary conditions would be less important than for low velocity impact.

Studies of the effect of impact location on panel response, of the effect of panel size and thickness on failure mode, and a comparison between test data and predictions were previously reported in Ref. 19.

The impact analysis program was used to compare a predicted delamination size with the results of several impact tests done by Byers.[20] Graphite-epoxy panels of the configuration shown in Fig. 12 were impacted with a four-pound weight at impact energies of 6.8, 11.3, and 15.8 J (60, 100, and 140 in.-lb) and C-scanned to determine the delamination size. Figure 12 shows the calculated variation of normal shear force across the panel for each impact test condition. Also shown in Fig. 12 are horizontal lines corresponding to interlaminar shear stresses of 34.5 and 68.9 MPa (5000 and 10,000 psi). If it is assumed that delamination would occur wherever the shear stress is greater than the allowable, then the predicted delamination size can be read from each curve. The measured and predicted delamination sizes for the test conditions are given in Table 1. It can be seen that for an interlaminar shear strength of 34.5 MPa (5000 psi) the best correlation with test data occurs, while static tests of short beam shear specimens in this laminate typically have interlaminar shear strengths of 68.9 MPa (10,000 psi). This difference can be explained by hypothesizing that the delamination starts at a stress of 68.9 MPa (10,000 psi) and grows dynamically until it is arrested at a lower value of about 34.5 MPa (5000 psi). As a further examination of dynamic effects, Fig. 13 shows a plot of impact energy vs delamination size for several impact tests.[21] There is no delamination at the lowest impact energy, [0.56-1.13 J (5-10 in.-lb)] while there is a large amount of delamination [greater than 10.2 mm (0.4 in.)] at the next higher impact energy. This sudden appearance of large areas of delamination is consistent with the hypothesis for dynamic delamination just described, in that there would be no delamination until the peak stress reached is above a threshold for the onset of growth [about 68.9 MPa (10,000 psi)] and the delamination would continue to grow until the stress had dropped below an arrest value [approximately 34.5 MPa (5000 psi)].

Conclusions

The equations presented in this paper allow an orthotropic panel to be analyzed for dynamic loads with only a little more effort than is required for a static analysis. A Basic language program has been developed for the Tektronix 4051 desktop computer incorporating the different loading pulses given by Eqs. (31-35). Thus, a dynamic analysis may be done without the necessity of resorting to approximate design curves and arbitrary dynamic magnification factors.

References

[1] Lekhnitskii, S. G., *Anisotropic Plates*, translated by S. W. Tsai and T. Cheron, Gordon and Breach, 1968.

[2] Ambartsumyan, S. A., *Theory of Anisotropic Plates*, translated by T. Cheron, edited by J. E. Ashton, Technomic, Stamford, Conn., 1969.

[3] Jones, R. M., *Mechanics of Composite Materials*, Scripta, Wash., 1975.

[4] Whitney, J. M. and Leissa, A. W., "Analysis of a Simply-Supported Laminated Anisotropic Rectangular Plate," *AIAA Journal*, Vol. 7, Jan. 1970, pp. 28-33.

[5] Ashton, J. E. and Whitney, J. M., *Theory of Laminated Plates*, Technomic, Stamford, Conn., 1970.
[6] Whitney, J. M. and Pagano, N. J., "Shear Deformation in Heterogeneous Anisotropic Plates," *Journal of Applied Mechanics*, Vol. 37, 1970, pp. 1031-1036.
[7] Mindlin, R. D., "Influence of Rotatory Inertia and Shear on Flexural Motions of Isotropic Elastic Plates," *Journal of Applied Mechanics*, Vol. 18, March 1951, pp. 31-38.
[8] Mierovitch, L., *Analytical Methods in Vibrations*, MacMillan, London, 1967.
[9] Warburton, G. B., *The Dynamical Behaviour of Structures*, Pergamon Press, Oxford, 1964.
[10] Yu, Y. Y., "Forced Flexural Vibrations of Sandwich Plates in Plane Strain," *Journal of Applied Mechanics*, Vol. 27, May 1960, pp. 535-540.
[11] Sun, C. T. and Whitney, J. M., "Forced Vibrations of Laminated Composite Plates in Cylindrical Bending," *Journal of the Acoustical Society of America*, Vol. 55, May 1974, pp. 1003-1008.
[12] Whitney, J. M. and Sun, C. T., "Transient Response of Laminated Composite Plates Subjected to Transverse Dynamic Loading," *Journal of the Acoustical Society of America*, Vol. 61, Jan. 1977, pp. 101-104.
[13] Sun, C. T. and Chattopadhyay, S., "Dynamic Response of Anisotropic Plates Under Initial Stress Due to Impact of a Mass," *Transactions of the ASME, Journal of Applied Mechanics*, Vol. 42, Sept. 1975, pp. 693-698.
[14] Timoshenko, S. P. and Woinowsky-Krieger, S., "Theory of Plates and Shells," 2nd ed., McGraw-Hill, New York, 1961.
[15] Glasstone, S., "The Effects of Nuclear Weapons," U.S. Government Printing Office, Washington, revised ed., 1964.
[16] Timoshenko, S. P., "Zur Frage Nach der Wirkung Eines Stosses auf einer Balken," *Zeitschrift für Mathematik und Physik*, Vol. 62, No. 2, 1913, p. 198.
[17] Goldsmith, W., *Impact*, Edward Arnold Ltd., London, 1960.
[18] Sun, C. T. and Lai, R.Y.S., "Exact and Approximate Analysis of Transient Wave Propagation in an Anisotropic Plate," *AIAA Journal*, Vol. 12, Oct. 1974, pp. 1415-1417.
[19] Dobyns, A. L. and Porter, T. R., "A Study of the Structural Integrity of Graphite Composite Structure Subjected to Low Velocity Impact," Paper 17-B presented at 35th Annual Conference of the Reinforced Plastics/Composites Institute, New Orleans, La., Feb. 1980.
[20] McCarty, J. (program manager), "Evaluation of Durability and Damage Tolerance of Composite Structures Suitable for Commercial Transport Aircraft," Boeing Commerical Airplane Company, Contract NAS 15107, 1978.
[21] Porter, T. R., personal communication, Boeing Military Airplane Company, Seattle, Wash., May 1979.